


# Qudit Entanglers Using Quantum Optimal Control

Sivaprasad Omanakuttan<sup>1,\*</sup>, Anupam Mitra,<sup>1</sup> Eric J. Meier,<sup>2</sup> Michael J. Martin,<sup>2,1</sup> and Ivan H. Deutsch<sup>1,†</sup>

<sup>1</sup>Center for Quantum Information and Control (CQuIC), Department of Physics and Astronomy, University of New Mexico, Albuquerque, New Mexico 87131, USA

<sup>2</sup>Materials Physics and Applications Division, Los Alamos National Laboratory, Los Alamos, New Mexico 87545, USA

 (Received 22 December 2022; accepted 30 October 2023; published 29 November 2023)

We study the generation of two-qudit entangling quantum logic gates using two techniques in quantum optimal control. We take advantage of both continuous, Lie algebraic control and digital, Lie group control. In both cases, the key is access to a time-dependent Hamiltonian, which can generate an arbitrary unitary matrix in the group  $SU(d^2)$ . We find efficient protocols for creating high-fidelity entangling gates. As a test of our theory, we study the case of qudits robustly encoded in nuclear spins of alkaline earth atoms and manipulated with magnetic and optical fields, with entangling interactions arising from the well-known Rydberg blockade. We applied this in a case study based on a  $d = 10$  dimensional qudit encoded in the  $I = 9/2$  nuclear spin in  $^{87}\text{Sr}$ , controlled through a combination of nuclear spin resonance, a tensor ac-Stark shift, and Rydberg dressing, which allows us to generate an arbitrary symmetric entangling two-qudit gate, such as CPhase. Our techniques can be used to implement qudit entangling gates for any  $2 \leq d \leq 10$  encoded in the nuclear spin. We also studied how decoherence due to the finite lifetime of the Rydberg states affects the creation of the CPhase gate and found, through numerical optimization, a fidelity of 0.9985, 0.9980, 0.9942, and 0.9800 for  $d = 2$ ,  $d = 3$ ,  $d = 5$ , and  $d = 7$ , respectively. This provides a powerful platform to explore the various applications of quantum information processing of qudits, including metrological enhancement with qudits, quantum simulation, universal quantum computation, and quantum error correction.

DOI: [10.1103/PRXQuantum.4.040333](https://doi.org/10.1103/PRXQuantum.4.040333)

## I. INTRODUCTION

In the standard paradigm of quantum information processing (QIP) one encodes information in qubits, the quantum analog of classical bits, by isolating two well-chosen energy levels of the system. In many platforms, one has access and control over multiple levels, which can enhance our ability to do QIP in a variety of ways [1–5]. In particular, one can encode information in base- $d > 2$  using  $d$ -level qudits [1]. With a larger state space per subsystem, qudits offer potential advantages for quantum communication [6], quantum algorithms [7–10], and topological quantum systems [11–13]. Quantum computation with qudits can also reduce circuit complexity and can

be advantageous in a variety of noisy intermediate-scale quantum (NISQ)-era applications [8–10, 14–17].

Qudits may also provide significant advantages in quantum error correction and fault-tolerant quantum computation [18–22]. Of particular importance is reducing the physical resources needed to encode logical qubits. In the standard paradigm, logical qubits are encoded in multiple physical qubits, such as in the well-known surface code [23], which has a substantial overhead. An alternative approach is to encode a logical qubit in a single qudit. This has been a powerful tool, e.g., in encoding a logical qubit in the multiple harmonic levels of a bosonic mode [5], and has been theoretically considered in high-dimensional spin qudits in atoms [3, 24], molecules [25], and in solid-state devices [26]. Developing general methods for quantum control and entanglement of qudits would greatly expand the tools at our disposal.

In the gate-based approach to quantum computation with qubits, a universal gate set consists of single-qubit gates that generate the group  $SU(2)$  and one entangling two-qubit gate, such as CNOT [27]. This generalizes simply for qudits. The universal gate set consists of the generators

\*somanakuttan@unm.edu

†ideutsch@unm.edu

Published by the American Physical Society under the terms of the [Creative Commons Attribution 4.0 International](https://creativecommons.org/licenses/by/4.0/) license. Further distribution of this work must maintain attribution to the author(s) and the published article's title, journal citation, and DOI.

of single-qudit gates in  $SU(d)$  and an entangling two-qudit gate [28–30]. Unlike qubits, where native Hamiltonians can be used to naturally implement the desired gate set, qudits require more complex protocols. The gates that are necessary for the implementation of the universal gate set have been recently implemented for qudits in superconducting transmon [2,31,32] as well as in trapped ions [33,34] up to dimension  $d = 7$ . In these experiments, one implements qudit gates using constructive methods through a prescribed set of Givens rotations [30,35]. While there has been substantial progress, much work remains to be done to efficiently implement a high-fidelity universal qudit gate set.

In this paper, we study an alternative approach based on quantum optimal control. Quantum optimal control was originally developed in NMR [36] and for coherent control of chemistry [37,38], and has been extensively used in quantum information processing [39]. We consider both continuous Hamiltonian control (Lie algebraic) and digital gate-based control (Lie group). Quantum optimal control has been experimentally implemented in a wide range of platforms ranging from ion traps [40], neutral atoms [41–43], superconductors [44,45], and nitrogen vacancy (N-V) centers [46,47]. Its use in implementing single-qudit gates was demonstrated in the seminal experiments of Jessen [48] with information encoded in the hyperfine states of cesium and studied in Ref. [49] for qudits encoded in the nuclear spin of alkaline-earth atoms. In this work, we extend these techniques to the implementation of entangling gates between two qudits. We study qudit entangling gates for any  $k \leq d$  within the  $d$ -dimensional Hilbert space of each subsystem.

As a concrete example that demonstrates the power of the method, we present here an optimal control scheme to implement entangling gates in qudits encoded in the nuclear spin of  $^{87}\text{Sr}$  atoms. The nuclear spin is a good memory for use in quantum information processing given its weak coupling to the environment and resilience to other background noise [50–52]. The ground state of the  $^{87}\text{Sr}$  is also studied in a recent paper as a possible candidate for qudit encoding with entangling interaction enabled by the Rydberg blockade [53]. Also, the recent significant achievements of quantum information processing using the Rydberg blockade [54–56] make this an ideal platform for exploring quantum computation. Using a combination of a tunable radio-frequency magnetic field and interactions that arise when atoms are excited to high-lying Rydberg states, the atomic qudit is fully controllable. We find that one can use quantum optimal control to implement high-fidelity entangling qudit gates even in the presence of decoherence arising from the finite Rydberg-state lifetime.

The remainder of this paper is organized as follows. In Sec. II we review the fundamentals of quantum control and define two approaches: Lie algebraic and Lie group theoretic protocols for the generation of any

arbitrary qudit entangling gates. In Sec. III, we study how control is achieved using numerical optimization based on the well-known GRAPE algorithm [57] and obtain control waveforms using the Lie algebraic method. We also use a gradient-based approach to find a digital sequence of unitary maps that achieves the desired gate using a Lie group theoretic method. Finally, we study how decoherence affects the fidelity of these gates. We give conclusions and outlook of our approach in Sec. IV.

## II. CONTROLLABILITY

A complete universal gate set for qudits requires one entangling gate. A standard choice is the CPhase gate, which is the generalization of CZ gate for qubits, defined

$$\text{CPhase} |j\rangle |k\rangle = \omega^{jk} |j\rangle |k\rangle, \quad (1)$$

where  $\omega = \exp(2\pi i/d)$ , the  $d$ th primitive root of identity for a subsystem of dimension  $d$ . We can see that for  $d = 2$  we recover the CZ gate. This gate is locally equivalent to the qudit-analog of the CNOT gate, known as the CSUM gate,

$$C_{\text{SUM}} |i\rangle |j\rangle = |i\rangle |i \oplus j \pmod{d}\rangle \quad (2)$$

by the Hadamard gate for qudits,  $H_d |j\rangle = 1/\sqrt{d} \sum_i \omega^{ij} |i\rangle$ . Previous works have studied how to implement these gates through a well-defined sequence of maps generated by one-qudit and two-qudit Hamiltonians [28,30,58,59]. We study here the use of numerical optimization and the theory of optimal control.

### A. Lie algebraic approach

In the Lie algebraic approach to quantum control, we consider a Hamiltonian of the form  $H[\mathbf{c}(t)] = H_0 + \sum_{j=1}^k c_j(t) H_j$ , where  $\mathbf{c}(t) = \{c_j(t)\}$  is the set of time-dependent classical control waveforms, and  $H_0$  is called the drift Hamiltonian. The system is said to be “controllable” if the set of Hamiltonians,  $\{H_0, H_1, H_2, \dots, H_k\}$ , are generators of the desired Lie algebra, e.g.,  $\mathfrak{su}(d)$ . Then  $\exists \mathbf{c}(t)$  such that  $U[\mathbf{c}, T] = \mathcal{T} \left[ \exp \left( -i \int_0^T H[\mathbf{c}(t)] dt \right) \right] = U_{\text{tar}}$  for any target unitary in desired Lie Group, e.g.,  $U_{\text{tar}} \in SU(d)$ . In addition, we require  $T \geq T_*$ , where  $T_*$  is known as the “quantum speed limit time,” which sets the minimal time needed for the system to be fully controllable.

We consider here open-loop control determined by a well-defined Hamiltonian of the general form,

$$H(t) = H^{(1)}(t) + H^{(2)}(t) + H_{\text{ent}}, \quad (3)$$

where  $H^{(i)}(t)$  are time-dependent Hamiltonians acting on the individual subsystems, and  $H_{\text{ent}}$  is the interaction that entangles them. Here we include the time dependence in the Hamiltonian that acts on the individual system as these

will be generally easier to implement experimentally. In this formulation,  $H_{\text{ent}} = H_0$ , is the drift Hamiltonian. However, one could in principle include time dependence in the entangling Hamiltonian as well and this may achieve faster gates.

### B. Lie group approach

In the digital, Lie group approach to quantum control, we consider a family of unitary maps in the desired group that are easily implementable,  $U(\lambda_j)$ , where  $\{\lambda_j\}$  are the parameters that specify the unitary matrices at our disposal. The relevant Lie group of interest here is  $SU(d^2)$ , the group of two-qudit unitary matrices in  $d^2$  dimensions, where the overall phase is removed. The system is controllable if  $\forall U_{\text{tar}} \in SU(d^2), \exists \{\lambda_j\}$  such that  $\prod_{j=1}^k U(\lambda_j) = U_{\text{tar}}$ . Similar to the Lie algebraic quantum control approach, the goal is to find  $\{\lambda_j\}$  through numeric optimization, e.g., via gradient-based methods.

For the case of two-qudit gates, a controllable Lie group structure is given as,

$$U_{\lambda_j} = U_{\text{ent}} * (U_1 \otimes U_2), \quad (4)$$

where  $U_{1,2} \in SU(d)$  and  $U_{\text{ent}} = \exp(-iH_{\text{ent}}t) \notin SU(d) \otimes SU(d)$ . Thus, we can achieve the target gate to the desired fidelity by intertwining a sequence of local  $SU(d)$  gates and the available entangling interaction in alternating layers of single-qudit gates and entangling gates, as shown in Fig. 1(b). This approach is similar to the construction based

on Givens rotation [33]. Here, the possibility of accessing arbitrary local  $SU(d)$  gates makes this protocol very powerful. A schematic comparison of both these approaches is shown in Fig. 1.

### C. Physical platform: Rydberg atoms

To make these ideas concrete, we consider the implementation of entangling gates in neutral atoms using the strong van der Waals interactions between atoms in high-lying Rydberg states. We use the Rydberg dressing paradigm in which one adiabatically superposes the Rydberg state into the ground states to introduce interactions between dressed ground states [60–65]. Rydberg dressing has been studied with multiple applications including the dynamics of interacting spin models [63–65] as well as to prepare metrologically useful states [66]. Entanglement between neutral atoms via Rydberg dressing has been theoretically proposed for creating qubit entangling gates [61,67,68] and experimentally implemented [62,69,70]. The dressing approach has a potential advantage in that it exhibits reduced sensitivity to some noise sources [61,67,70]. For the specific protocol based on optimal control, the utilization of Rydberg dressing confines our operations to the qudit subspace. This restriction effectively reduces the dimension of the Hilbert space for optimization from  $(2d)^2$  to  $d^2$  for a  $d$ -dimensional qudit. This dimension reduction significantly accelerates the numerical optimization of the pulses required for quantum control.

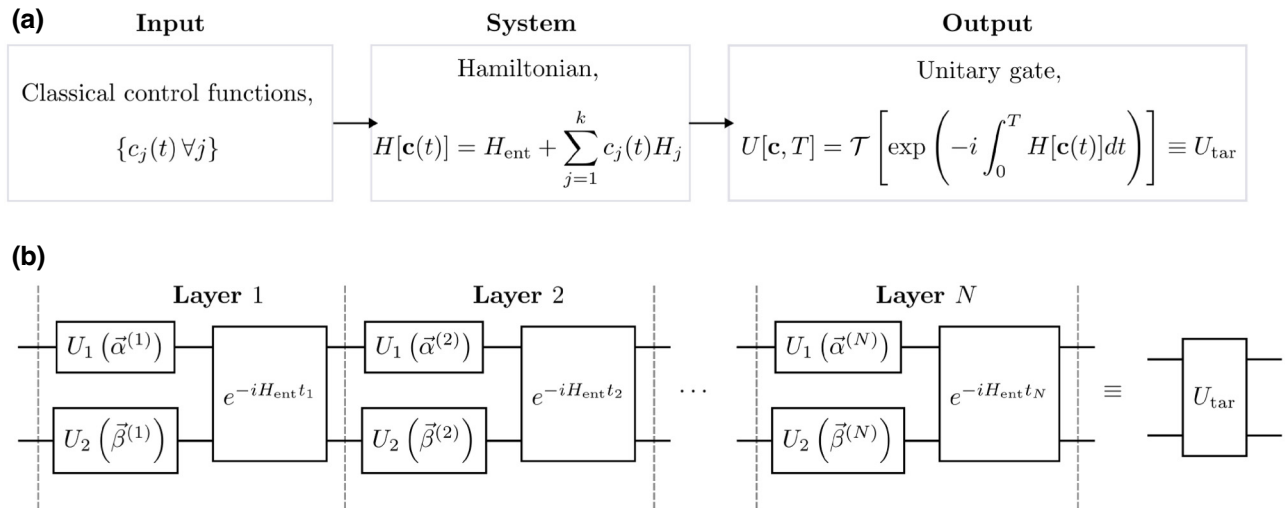


FIG. 1. Comparison of Lie algebra versus Lie group approach for quantum control. (a) Schematic of the continuous-time Lie algebraic approach for quantum control. The physical systems are governed by the time-dependent Hamiltonian,  $H[\mathbf{c}(t)] = H_{\text{ent}} + \sum_{j=1}^k c_j(t)H_j$ , here with a time-dependent entangling Hamiltonian,  $H_{\text{ent}}$ . The time-dependent waveforms  $\{c_j(t)\}$  are found through numerical optimization, and this defines the target unitary map of interest through the solution to the time-dependent Schrödinger equation. (b) Schematic for a digital, Lie group approach to quantum control of entangling two-qudit gates. The target unitary is achieved through a discrete series of layers consisting of unitary maps from a given family. One layer of the scheme consists of single-qudit gates on each subsystem and an entangling interaction between them, applied for a given time  $t_j$ . Through numerical optimization, one finds the parameters of the local  $SU(d)$  gates and the entangling time  $t_j$  in each layer.

We study here encoding a qudit in the spin of  $^{87}\text{Sr}$ . In the ground state, there is neither orbital nor spin angular momentum in the electrons,  $J = 0$ , and only nuclear spin,  $I = 9/2$ , giving us ten possible levels in which to encode our qudit, labeled from  $|0\rangle = |m_I = 9/2\rangle, |1\rangle = |m_I = 7/2\rangle, \dots, |9\rangle = |m_I = -9/2\rangle$ . The nuclear spin is highly isolated from the environment and thus serves as a robust memory for quantum information. In Ref. [49] we studied how we could implement single-qudit gates in these systems through a combination of a laser-induced tensor light shift and rf-induced Larmor precession. We generalize to the two-qudit case here.

To implement entangling two-qudit control, we will make use of the excitation to the  $5s5p^3S_1$  Rydberg series from one of the metastable  $5s5p^3P_J$  first excited states in the triplet series. For optimal control based on the combination of rf-driven Larmor precession and Rydberg dressing one can compare different choices of metastable states. One natural choice is the  $^3P_0$  clock state, whose spin is essentially solely nuclear, and thus robust in the presence of magnetic field noise. By contrast, the  $^3P_2$  state involves electronic angular momentum with a large magnetic dipole moment and commensurate sensitivity to noise, including possible tensor light shifts induced by the trapping laser. However, within the specific approach addressed in this study, access to a large magnetic dipole moment enables faster gate operations compared to the Rydberg lifetime. For the  $^3P_2$  states, the strength of the rf-Larmor precession frequency is closer to that of the available Rydberg dressing interaction. In this regime, the quantum speed limit (i.e., the minimum time required to implement gates) is more favorable compared to the situation that the rf interaction is much weaker than the Rydberg interaction, as would be the case for the  $^3P_0$  states. This regime, characterized by similar strengths of competing Hamiltonians, is known to be optimal for achieving the quantum speed limit [49,71]. We consider here coherently transferring qudits from the  $^1S_0$  ground state to the  $F = 9/2$  state hyperfine states of the  $^3P_2$  manifold, which provides for faster and more flexible control [72], putting technical noise aside.

To achieve the entangling interaction, we consider Rydberg dressing, generalizing the mechanism discussed in Refs. [61,62,67]. The ac Stark shift (light shift) associated with a dressed state when a laser is tuned near a Rydberg resonance is modified for two atoms because of the Rydberg blockade. The deficit between the two-atom light shift and twice the one-atom light shift determines the entangling energy [61]. For the case of qudits, the same physics holds, but now with a multilevel structure and a spectrum of entangling energies. When the spectrum is nonlinear, the system is controllable.

Figure 2 depicts the basic scheme. Those levels of the qudit that we chose to participate in the gate are excited from the ground  $^1S_0$  to the first excited  $^3P_2$  state.

The Rydberg states in  $^{87}\text{Sr}$  have well-resolved hyperfine splitting. We consider UV dressing laser near the resonance between the  $^3P_2, F = 9/2$  hyperfine manifold and the  $^3S_1, F' = 11/2$  Rydberg hyperfine states. In the presence of a bias magnetic field, due to the difference in the  $g$  factors, the two manifolds will be differently Zeeman shifted. The different magnetic sublevels that define the qudit will thus be differently detuned to the Rydberg magnetic sublevels. Due to this and the Clebsch-Gordan coefficients associated with the different transitions, each sublevel will be differently dressed (equivalently, there is a tensor light shift). When two atoms are dressed, the effect of the Rydberg blockade modifies the spectrum as discussed above.

An example of two sublevels (one from each atom) is shown in Fig. 2(b). Diagonalizing this atom-laser Hamiltonian under the approximation of a perfect Rydberg blockade yields the representation

$$H_{\text{ent}} = \sum_{ij} E^{ij} |\tilde{ij}\rangle \langle \tilde{ij}|, \quad (5)$$

where the tilde indicates dressed states,

$$|\tilde{ij}\rangle = C_{ij} |ij\rangle + C_{rj} |rj\rangle + C_{irj} |irj\rangle, \quad (6)$$

and  $E^{ij}$  are the light shifts originating from these interactions. The spectrum of the entangling Hamiltonian shown in Fig. 2(c) gives us insight into the controllability of the system. In the chosen order, the spectrum reveals the structure of ten quadratic potentials arising from a combination of the tensor light shift and Rydberg blockade. This nonlinearity makes the Hamiltonian controllable; further details are discussed in Appendix B.

The time-dependent Hamiltonian necessary for the Lie algebraic control can be chosen as phase-modulated Larmor precession,  $H_{\text{mag}} = -\boldsymbol{\mu} \cdot \mathbf{B}(t)$ , with  $\boldsymbol{\mu} = g_F \mu_B \mathbf{F}$  the magnetic dipole vector operator, and where  $\mathbf{B}(t) = B_{\parallel} \mathbf{e}_z + B_T \text{Re}[(\mathbf{e}_x + i\mathbf{e}_y) e^{-i(\omega_{\text{rf}} t + \phi(t))}]$ . Defining the auxiliary subspace,  $a$ , for the levels in hyperfine manifold  $\{5s5p^3P_2, F = 9/2\}$  and the subspace,  $r$ , for the levels  $\{5s5p^3S_1, F' = 11/2\}$  in the Rydberg hyperfine manifold, we have  $g_F(r)/g_F(a) \approx 2$ . Thus defining the Zeeman shift  $\omega_0 = g_F(a)B_{\parallel}$ , the Larmor precession frequency  $\Omega_{\text{rf}} = g_F(a)B_T$ , and choosing rf drive on resonance in the  $a$  manifold,  $\omega_{\text{rf}} = \omega_0$ , in the co-rotating frame at  $\omega_0$ , the Hamiltonian is

$$\begin{aligned} H_{\text{mag}}^{(a)}(t) &= \Omega_{\text{rf}} \left[ \cos \phi(t) F_x^a + \sin \phi(t) F_y^a \right], \\ H_{\text{mag}}^{(r)}(t) &= 2\Omega_{\text{rf}} \left[ \cos \phi(t) F_x^r + \sin \phi(t) F_y^r \right] + \omega_0 F_z^r, \end{aligned} \quad (7)$$

where  $F_i^a, F_i^r$  are the spin angular momentum operators in the respective subspaces along axis  $i \in \{x, y, z\}$ .

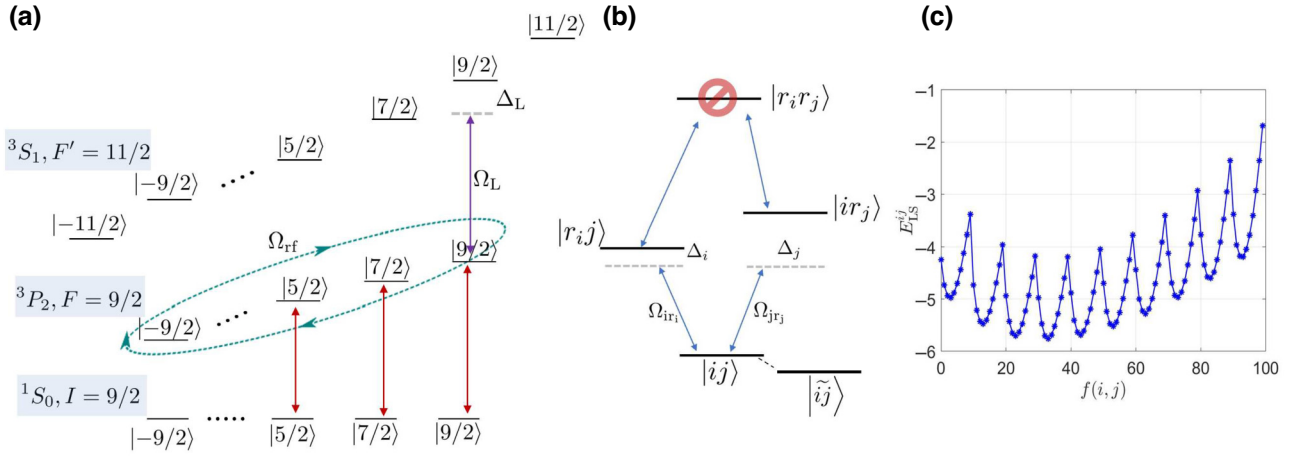


FIG. 2. Schematic for designing two-qudit entangling interactions in  $^{87}\text{Sr}$  neutral atoms. (a) A  $k \leq d$ -dimensional qudit is encoded in memory in the nuclear spin with  $d = 10$  magnetic sublevels in the electronic ground state ( $5s^2$ )  $^1S_0$ . When the gate is to be performed, the  $k$  levels (here  $k = 3$ ) are transferred coherently to the metastable clock states ( $5s5p$ )  $^3P_2, F = 11/2$  in the presence of a bias magnetic field. The system becomes controllably by adiabatically dressing the  $^3P_2$  with Rydberg character through the application of a near-resonant laser with Rabi frequency  $\Omega_L$  and detuning  $\Delta_L$  with respect to the hyperfine manifold ( $5sns$ )  $^3S_1, F' = 9/2$  in the Rydberg series. Control is then achieved through the application of a phase-modulated rf field with Rabi rate  $\Omega_{\text{rf}}$ , which acts on the dressed states to generate a nonlinear Larmor precession. The entanglement arises due to the Rydberg blockade. The coupling of the state of two qudits for a perfect blockade as depicted in (b), where  $i$  is a state from the first qudit and  $j$  is from the second qudit, excited by two Rabi frequencies and detunings determined by the Clebsch-Gordan coefficients and Zeeman shifts. The state  $|ij\rangle \rightarrow |\tilde{ij}\rangle$  is the dressed state given in Eq. (6). The spectrum of eigenvalues of the entangling Hamiltonian Eq. (5) is given in (c) as a function of  $i$  and  $j$  where the function chosen is  $f(i, j) = 10i + j$ ;  $0 \leq i, j < 10$ . The spectrum indicates ten parabolas, where each parabola corresponds to the effect of a single state in the first atom sees due to all the states in the second atom. This nonlinear spectrum arises through a combination of the tensor ac Stark shift and the Rydberg blockade, making the system controllable, allowing us to implement any symmetric two-qudit gate in this system of interest.

As the  $H_{\text{mag}}$  acts on the laser-dressed states defined in Eq. (6), which are superpositions of  $a$  and  $r$  states that have different  $g$  factors, one needs to find the action of the magnetic interaction in the dressed basis. Due to the nonlinearity, the action of the rf-magnetic driving on the dressed states is no longer simple Larmor precession. Considering a global rf-magnetic interaction, the  $H_{\text{mag}}$  acts on both qudits as

$$\begin{aligned} & (H_{\text{mag}}(t) \otimes \mathbb{1} + \mathbb{1} \otimes H_{\text{mag}}(t)) |\tilde{ij}\rangle \\ &= C_{ij} \left[ H_{\text{mag}}^{(a)}(t) \otimes H_{\text{mag}}^{(a)}(t) \right] |ij\rangle \\ &+ C_{rj} \left[ H_{\text{mag}}^{(r)}(t) \otimes H_{\text{mag}}^{(a)}(t) \right] |rj\rangle \\ &+ C_{ir_j} \left[ H_{\text{mag}}^{(a)}(t) \otimes H_{\text{mag}}^{(r)}(t) \right] |ir_j\rangle. \end{aligned} \quad (8)$$

Thus in the dressed basis, the Hamiltonian is  $H(t) = \tilde{H}[\phi(t)] + H_{\text{ent}}$ , where the action of the magnetic field in the dressed basis is given by the Hamiltonian,

$$\tilde{H}[\phi(t)] = \sum_{i,j,k,l} \langle \tilde{ij} | H_{\text{mag}}(t) \otimes \mathbb{1} + \mathbb{1} \otimes H_{\text{mag}}(t) | \tilde{kl} \rangle |\tilde{ij}\rangle \langle \tilde{kl}|. \quad (9)$$

By modulating the phase  $\phi(t)$  one can generate any target unitary gate.

### III. NUMERICAL METHODS

We consider encoding a  $k$ -dimensional qudit in the  $d = 10$  dimensional Hilbert space associated with ten magnetic sublevels of the nuclear spin of  $^{87}\text{Sr}$ . To implement gates based on optimal control for  $k < 10$ , we use techniques based on the structure of partial isometries. A partial isometry of dimension  $k \leq d$  in a physical system of dimension  $d$  is defined as,

$$V_{\text{tar}} = \sum_{i=1}^k |f_i\rangle \langle e_i|, \quad (10)$$

where  $\{|e_i\rangle\}, \{|f_i\rangle\}$  are two orthonormal bases for the qudit. The unitary of maps of interest then has the form,

$$U_{\text{tar}} = V_{\text{tar}} + V_{\perp}, \quad (11)$$

where  $V_{\perp}$  acts on the orthogonal subspace, with dimension  $d - k$ . To find the control waveform, one then optimizes the fidelity between the target isometry and the isometry

generated using quantum control [73]

$$\mathcal{F}_V[\mathbf{c}, T] = \left| \text{Tr} \left( V_{\text{tar}}^\dagger V[\mathbf{c}, T] \right) \right|^2 / k^2. \quad (12)$$

### A. Numerical results for Lie algebraic approach

As discussed in Sec. II C, one can implement an arbitrary entangling gate through a combination of Rydberg dressing and phase-modulated Larmor precession driven by rf fields. Because our control Hamiltonian is symmetric with respect to the exchange of the qudits, we consider here symmetric gates, with global control. We seek, through numerical optimization, the time-dependent rf phase,  $\phi(t)$ . To achieve this we employ the well-known GRAPE algorithm [57]. To implement GRAPE, we discretize the control waveform,  $\phi(t)$ , and numerically maximize the fidelity by gradient ascent. We choose here a piecewise constant parameterization (as in Ref. [48]) and write the control waveform as a vector  $\mathbf{c} = \{\phi(t_j)/\pi \mid j = 1, \dots, n\}$  where  $t = j \Delta t$  and  $n = T/\Delta t$ . The waveform is thus a series of square rf pulses with constant amplitude and phase over the duration  $\Delta t$ .

The minimum number of elements in the control vector  $\mathbf{c}$  is determined by the number of parameters needed to specify the target isometry. A  $K$ -dimensional partial isometry is defined by the  $K$  columns in a  $D \times D$ -dimensional unitary matrix. Hence, to find the number of free parameters for a  $K$ -dimensional isometry one can count the number of parameters needed to specify  $K$  orthonormal vectors uniquely in a  $D$ -dimensional vector space. This is given by

$$\begin{aligned} n_{\min}(K, D) &= \sum_{j=1}^K 2(D-j) - 1 + K - 1 \\ &= 2 \left[ KD - \frac{K(K+1)}{2} \right] + K - 1 \\ &= 2KD - K^2 - 1, \end{aligned} \quad (13)$$

where in the first line, we subtracted one from the parameter count since the overall phase of the isometry is neglected. Equation (13) recovers well-known limits. When  $K = 1$  and  $D = d$ ,  $n_{\min} = 2d - 2$ , which is the number of free parameters needed to specify a pure state in a  $d$ -dimensional Hilbert space. When  $K = D = d$ ,  $n_{\min} = d^2 - 1$ , which is the number of free parameters needed to specify a special unitary map in  $d$  dimensions.

In the Lie algebraic protocol for designing entangling gates, the control Hamiltonian, as well as the target unitary matrices, are symmetric under the exchange of qudits. In this case, one can work in the symmetric subspace for two qudits. Using the hook length formula [74], the dimension of the symmetric subspace of the total vector space and

TABLE I. The minimum number of parameters required for encoding a partial isometry of dimension  $k$  in the  $d = 10$  dimensional Hilbert space according to Eq. (13) for the prime dimensions  $k \leq 10$  with  $K$  and  $D$  given by Eq. (14).

$k$	$n_{\min}(K, D)$
2	320
3	623
5	1424
7	2295

isometry is,

$$D = \frac{d(d+1)}{2}, K = \frac{k(k+1)}{2}. \quad (14)$$

Thus, using Eq. (13), we find the number of free parameters required for the two-qubit entangling unitary given in Table I.

Proof-of-principle numerical examples of waveforms that generate the CPhase gate are given in Fig. 3. The figure gives the  $\phi(t)$  as a piecewise constant function of time, obtained using the GRAPE algorithm. We consider prime-dimensional qudits, the cases of most interest in quantum algorithms. Figure 3(a) shows the case of the  $k = 3$ , a qutrit encoded in  $d = 10$ . The total time is  $T = 50\pi/\Omega_{\text{rf}}$ , which is divided into 700 intervals for the quantum control. Figure 3(b) shows an example waveform for the case of  $k = 5$ . Here, the total time is  $T = 240\pi/\Omega_{\text{rf}}$ , divided into 1600 intervals. Similarly, Fig. 3(c) shows the case of  $k = 7$  in our  $d = 10$  level system. The total time is  $T = 400\pi/\Omega_{\text{rf}}$ , divided into 2500 time intervals. This controllable Hamiltonian can also be used to generate other two-qudit gates. The qudit generalization of the Mølmer-Sørensen gate, as is given in Appendix C.

The waveforms found here are a proof-of-principle set of square pulses and are not intended to be taken as the best choice for experimental implementation. In practice, one can design and optimize for much smoother waveforms using well-known techniques by imposing additional constraints on bandwidth and slew rate. Alternatively, one can optimize in the Fourier domain or in any other complete basis of functions using the techniques of gradient optimization of analytic controls (GOAT) [75].

### B. Numerical results for Lie group approach

In the Lie group control protocol discussed in Sec. II C we parameterize the target unitary map as

$$\begin{aligned} U_{\text{tar}} &= \prod_j U_{\lambda_j}, \\ &= \prod_j e^{-iH_{\text{ent}} t_j} U_1(\vec{\alpha}^{(j)}) \otimes U_2(\vec{\beta}^{(j)}). \end{aligned} \quad (15)$$

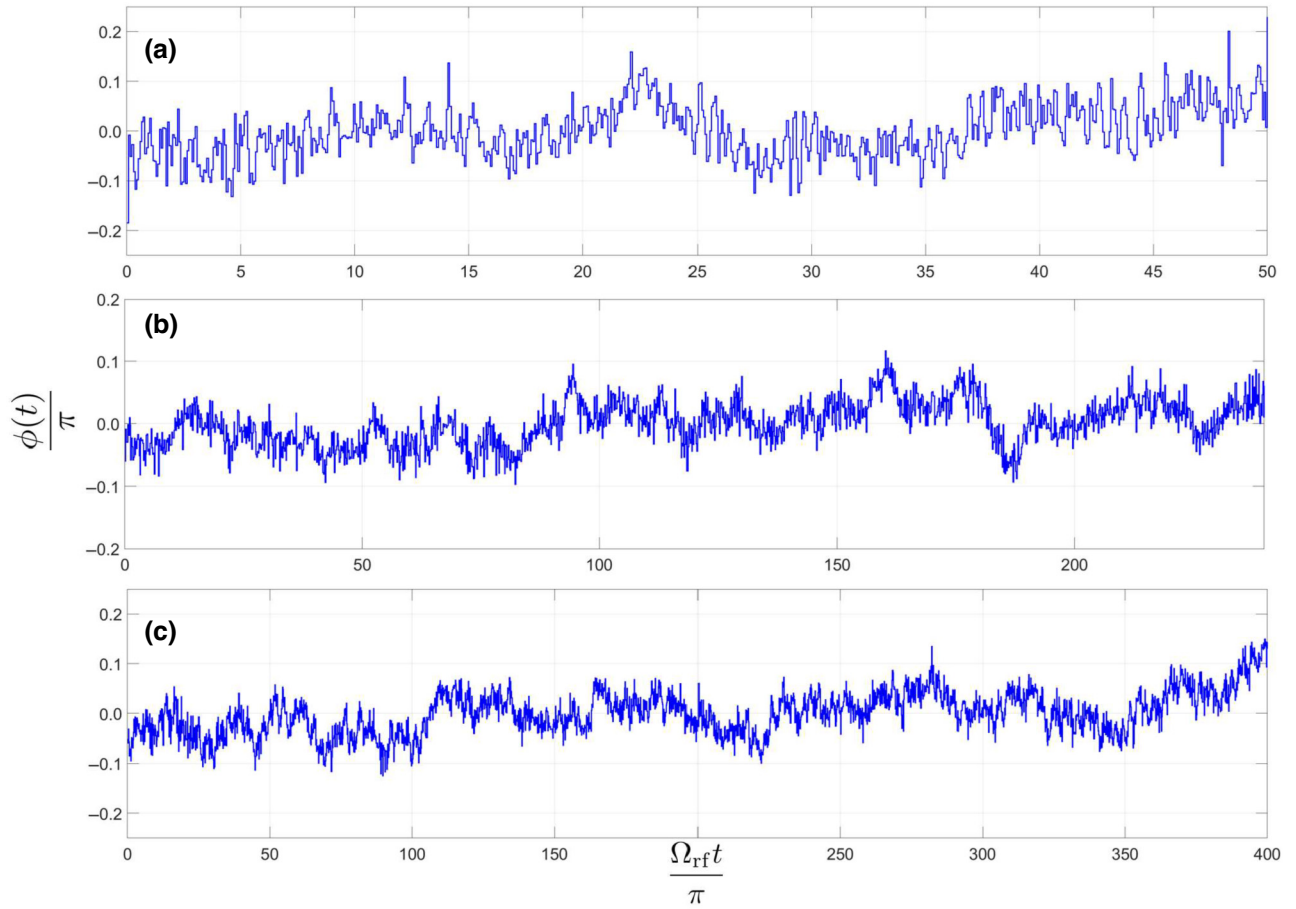


FIG. 3. Waveforms of the CPhase gate. Quantum control is achieved by modulating the phase of an rf field as a function of time,  $\phi(t)$ . We parameterize this by a piecewise constant waveform. The figure shows proof-of-principle examples of  $\phi(t)$  that generate the CPhase gate, optimized using the GRAPE algorithm for different qudit dimensions. (a) The case of the  $d = 3$  for a total time of  $T = 50\pi/\Omega_{\text{rf}}$  with 700 piecewise constant steps. (b) The case of the  $d = 5$  for a total time of  $T = 240\pi/\Omega_{\text{rf}}$  with 1600 piecewise constant steps. (c) The case of the  $d = 7$  for a total time of  $T = 400\pi/\Omega_{\text{rf}}$  with 2500 piecewise constant steps. For all of these calculations, the rf field is on resonance with the Zeeman splitting  $\omega_{\text{rf}} = \omega_0$  and we choose the rf-Larmor frequency  $\Omega_{\text{rf}} = \omega_{\text{rf}}$ . Control is achieved by Rydberg dressing with laser Rabi frequency  $\Omega_L = 6\Omega_{\text{rf}}$ .

The control parameters  $\{\lambda_i\}$  consist of the set of times  $\{t_i\}$  and the  $2(d^2 - 1)$  parameters  $\vec{\alpha}^{(j)}, \vec{\beta}^{(j)}$ , which specify each of the local  $\text{SU}(d)$  unitary maps. We can parameterize these according to

$$U_i(\vec{\alpha}^{(j)}) = \exp\left(-i \sum_{i=1}^{d^2-1} \alpha_i^{(j)} \Lambda_i\right), \quad (16)$$

where  $\Lambda$  is the generalized Gell-Mann matrices that span the Lie algebra  $\mathfrak{su}(d)$ . The matrices can be categorized as,

$$\begin{aligned} \text{symmetric: } \Lambda_{jk}^x &= |j\rangle\langle k| + |k\rangle\langle j|, \\ \text{antisymmetric: } \Lambda_{jk}^y &= -i|j\rangle\langle k| + i|k\rangle\langle j|, \\ \text{diagonal: } \Lambda_j^z &= \sum_{l=1}^l |j\rangle\langle j| - l|l+1\rangle\langle l+1|. \end{aligned} \quad (17)$$

The task of the numerical optimization, thus, is to find the set of times of the entangling interaction  $\{t_j\}$ , and the expansion coefficients of the Gell-Mann matrices  $\{\alpha_i^{(j)}\}$  and  $\{\beta_i^{(j)}\}$ . We denote this whole set of parameter as  $\{\lambda_j\} = \{t_j, \vec{\alpha}^{(j)}, \vec{\beta}^{(j)}\}$ .

We define one layer of the control as consisting of a pair of local  $\text{SU}(d)$  gates followed by the entangling Hamiltonian for a time  $t_j$ . The total number of free parameters for a CPhase gate is  $d^2(d^2 + 1)/2$ , as follows from Eq. (14) for a symmetric gate in  $\text{SU}(d^2)$ . Thus, the minimum number of layers required to obtain the CPhase gate is given by

$$\begin{aligned} N_{\min} (2(d^2 - 1) + 1) &= \frac{d^2(d^2 + 1)}{2} \\ N_{\min} &= \frac{d^2(d^2 + 1)}{2(2d^2 - 1)}. \end{aligned} \quad (18)$$

TABLE II. The number of layers of primitive gates in the Lie group approach required to achieve the CPhase gate. The theoretical minimum is  $N_{\min}$  according to Eq. (18). If we allow locally addressable single-qudit gates, the number of layers required is  $N_{\text{local}}$ . If we have only global control but allow for a sign change in the entangling Hamiltonian, the number of layers required is  $N_{\text{global}}$ .

$d$	$N_{\min}$	$N_{\text{local}}$	$N_{\text{global}}$
3	3	6	7
5	7	10	12
7	13	14	15

The numerical results for the minimum number of layers needed in the system are given in Table II for the cases of  $d = 3, 5$ , and  $d = 7$ . In practice, we find that one needs more than this minimum number of layers to implement the target unitary gate with high fidelity. This improves the optimization landscape for gradient ascent [76].

For our case under study, we choose the same entangling Hamiltonian as we used in the Lie algebraic approach given in Eq. (5). However, unlike that approach, we interleave the entangling interaction with local single-qudit  $SU(d)$  gates. Implementation of this requires another layer of optimization. As we do not have access to native Hamiltonians proportional to the Gell-Mann matrices, to implement local qudit gates we can employ local  $SU(d)$  optimal control [49]. From a practical perspective, this might be implemented directly in the  ${}^3P_2$  manifold, either through a combination of tensor-light shift and rf-driven Larmor precession similar to Ref. [49], or alternatively through a combination of microwave-driven Rabi oscillations between different hyperfine levels in  ${}^3P_2$  and rf-driven Larmor precession as in Ref. [48]. In either case, optimal control can be used to find the relevant experimental waveform that generates the desired local  $SU(d)$  gates.

In this analysis, we included locally addressable control on each qudit. Though the CPhase gate is symmetric under exchange, we find that this symmetry breaking is necessary for effective optimization of this parameterization, similar to that seen in Ref. [77]. An alternative protocol is to employ symmetric global control of the local unitaries,  $\vec{\alpha}^{(i)} = \vec{\beta}^{(i)}$ , but to reverse the sign of the entangling Hamiltonian  $H_{\text{ent}} \rightarrow -H_{\text{ent}}$  in alternating layers. This allows for effective optimization, and the corresponding result is given in Table II.

### C. Decoherence

In a closed quantum system, quantum optimal control employing either the Lie algebraic or the Lie group approaches can be used in principle to implement any qudit entangling gate to any desired fidelity. In our numerical optimization, we took the target infidelity to be  $10^{-3}$ . In the absence of decoherence, we could achieve that target

in a reasonable time for  $d \leq 5$ . For  $d = 7$ , more time is required. However, the fundamentally achievable fidelity is limited by decoherence associated with the particular physical platform. For the system at hand, decoherence occurs due to the finite lifetime of the Rydberg states, which predominantly leads to leakage and loss outside the computational basis. In that case, we can model the gate as generated by a non-Hermitian effective Hamiltonian,  $H_{\text{eff}}[c(t)]$ , where the Hermitian part is the control Hamiltonian and the anti-Hermitian represents decay out of the Rydberg states. The fidelity of interest is given by

$$\mathcal{F}_V[\mathbf{c}, T] = \left| \text{Tr} \left( V_{\text{tar}}^\dagger V_{\text{eff}}[\mathbf{c}, T] \right) \right|^2 / d^2, \quad (19)$$

where  $V_{\text{eff}}[\mathbf{c}, T] = \mathcal{T} \left[ \exp \left( -i \int_0^T H_{\text{eff}}[\mathbf{c}(t)] dt \right) \right]$ . Here the decay amplitude from a dressed state is  $\gamma_{\text{decay}}^{ij} = |C_{r_{ij}}|^2 \Gamma_{r_i} + |C_{i_{r_j}}|^2 \Gamma_{r_j}$ , which in turn gives the effective Hamiltonian as

$$H_{\text{ent}}^{\text{eff}} = \sum_{ij} \left( E_{\text{LS2}}^{ij} - i\gamma_{\text{decay}}^{ij}/2 \right) |\tilde{j}\rangle \langle \tilde{j}|. \quad (20)$$

With this model for decoherence in hand, the numerical results for the Lie algebraic approach are given in Fig. 4, which shows the infidelity as a function of time for a CPhase gate for different dimension isometries. We focus here on the case of the prime dimensional qudits. In contrast to closed-system control, in the presence of decoherence, infidelity decreases at first and then increases. This is due to the fact there is an optimal time of evolution, larger than the quantum speed limit, but not too large when compared to the coherence time of the system. As expected, one needs more time as the qudit dimension increases, which in turn results in an increase in the minimum infidelity one could achieve in each of these cases as shown in Fig. 4. We obtain a maximum fidelity of 0.9985, 0.9980, 0.9942, and 0.9800 for  $d = 2, d = 3, d = 5$ , and  $d = 7$ , respectively, for the CPhase gate. Note, the values of fidelity for different dimensional qudits should be considered in the context of a particular application. For example, the threshold for fault tolerance for qudits, in general, is larger for larger  $d$  [78,79]. For the particular scheme considered in Ref. [78], the threshold for  $d = 2, d = 3, d = 5$ , and  $d = 7$  are close to 0.008, 0.012, 0.0135, and 0.015, respectively. Hence, the proof-of-principle fidelity obtained here is promising and can be further optimized.

In the Lie group approach, we can use the effective Hamiltonian to describe the evolution when the Rydberg



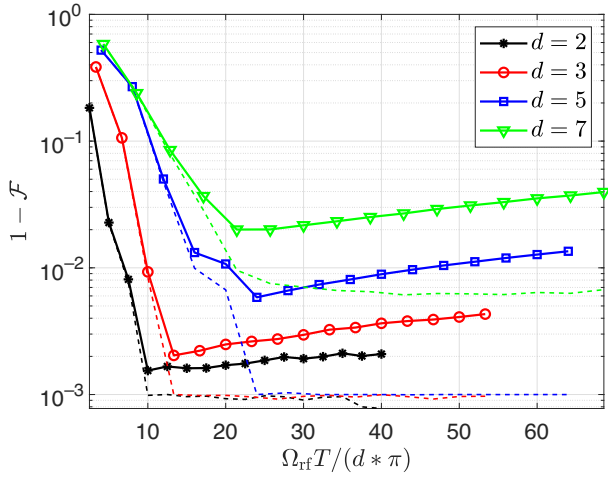


FIG. 4. Infidelity as a function of time. Simulated infidelity with and without decoherence as a function of control time divided by the dimension  $d$  for CPhase gate with different prime dimensions with  $d \leq 10$ , as found using Lie algebraic quantum control and the GRAPE algorithm. Decoherence due to Rydberg decay outside the computational basis is included through an imaginary part of the Hamiltonian. We take the Rydberg lifetime to be  $140 \mu\text{s}$  and choose the rf-Larmor frequency to be  $\Omega_{\text{rf}}/2\pi = 10 \text{ MHz}$ . In the absence of decoherence (dashed lines), for a time greater than the “quantum speed limit” (the time required to obtain ideal fidelity) we achieve a minimal error (infidelity) of  $10^{-3}$  due to our threshold in the numerics for  $d \leq 5$ . This speed-limit time increases as we increase the qudit dimension, which in turn results in an increased decay in maximum fidelity. For the CPhase gate, we obtain a fidelity of 0.9985, 0.9980, 0.9942, and 0.9800 for  $d = 2, d = 3, d = 5$ , and  $d = 7$ , respectively. For all of these calculations, we have taken the dressing laser Rabi frequency to be  $\Omega_L = 6\Omega_{\text{rf}}$  and the lifetime of the Rydberg states to be  $140 \mu\text{s}$ .

dressing is employed. In this case, we have,

$$\begin{aligned} U_{\text{tar}}^{\text{eff}} &= \prod_j U_{\lambda_j}, \\ &= \prod_j e^{-iH_{\text{ent}}^{\text{eff}} t_j} U_1(\vec{\alpha}^{(j)}) \otimes U_2(\vec{\beta}^{(j)}). \end{aligned} \quad (21)$$

We neglect here any decoherence associated with the local  $SU(d)$  gates. Thus the fidelity including the decoherence effects is given as,

$$\mathcal{F}_{\text{eff}} = \left| \text{Tr} \left( U_{\text{tar}}^{\dagger} U_{\text{tar}}^{\text{eff}} \right) \right|^2 / d^2. \quad (22)$$

A comparison of the fidelities achieved based on the Lie algebraic and Lie group approaches is given in Fig. 5 for  $d = 3, 5$ , and  $d = 7$ . The results suggest that the Lie algebraic protocol slightly outperforms the Lie group protocol in the presence of decoherence. This difference in the performance can be attributed to the time spent in the

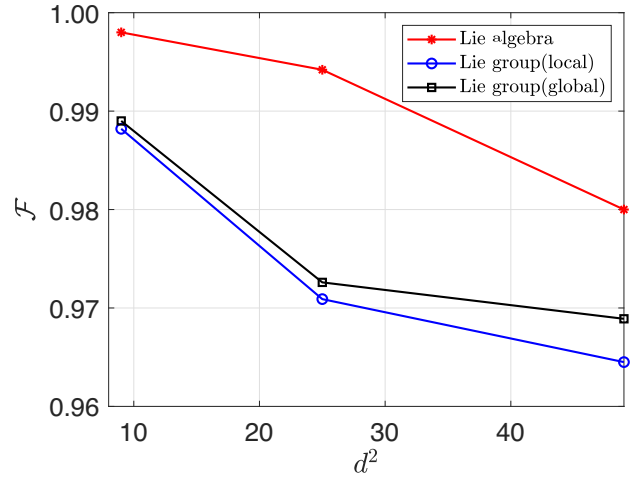


FIG. 5. A comparison of the optimized fidelity,  $\mathcal{F}$  of the CPhase gate achieved for the Lie algebraic and Lie group approaches (including both local single-qudit control and only global control) is plotted as a function of the total Hilbert space dimension  $d^2$ , for the qudits of dimension  $d = 3, 5$ , and  $d = 7$ . For all of these simulations, we have taken the parameters given in Fig. 4.

Rydberg state for these two approaches, as shown in Fig. 6. Fundamentally, we can understand this from the fact that the Lie algebraic approach has more control parameters as compared to the Lie group protocol. Thus, based on the Magnus expansion [80–82], the nested commutators, which are at the heart of controllability, become easier to achieve. Both approaches yield high fidelities in large dimensional qudits. Nevertheless, the Lie group approach may be preferable when considering the complexity necessary for experimental control. The difference in the behavior of Lie group (local) to Lie group (global) is due to the fact that for the global approach we allow  $H_{\text{ent}} \rightarrow -H_{\text{ent}}$  in alternating layers.

In general, a key experimental consideration for the successful implementation of open-loop quantum control is the effect of uncertainties in Hamiltonian parameters. These can be mitigated to some degree using the tools of robust quantum control [83–86]. Such techniques are generalizations of spin-echo type composite pulses, which can be useful when there is sufficient coherence time. With a detailed understanding of the dominant inhomogeneities, robust optimal control can be used to implement suitable composite waveforms for qudit entanglers on any platform.

The specific experimental foundation of this proposal is well motivated by the existing literature, particularly the work of the Jessen group [48]. One particular issue discussed above is the trap-induced differential light shifts between the ground state and excited state  $^3P_2$  manifold [87]. It will be necessary to mitigate motional dephasing arising from vector and tensor shifts, which induce an

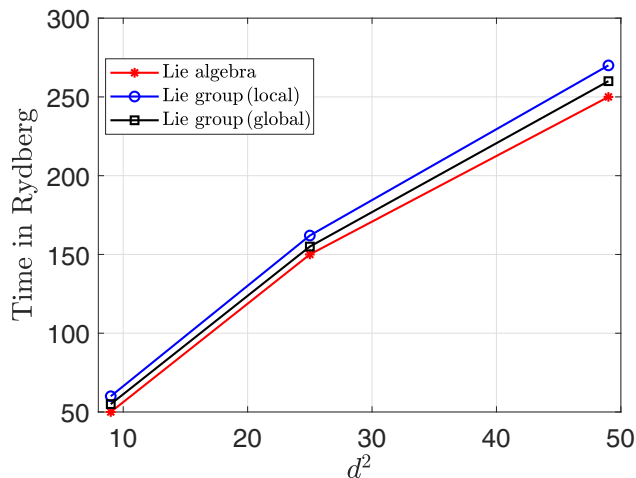


FIG. 6. A comparison of the minimum time spent in the Rydberg state to implement the CPhase gate achieved for the Lie algebraic and Lie group approaches (including both local single-qudit control and only global control) is plotted as a function of the total Hilbert space dimension  $d^2$ , for the qudits of dimension  $d = 3, 5$ , and  $d = 7$ . For all of these simulations, we have taken the parameters given in Fig. 4. Thus the time required for the Lie algebraic control is smaller than the Lie group control, which in turn contributes to the fidelity.

$m_F$  dependence on polarizability, thus inducing possible motional dephasing between  $m_F$  levels. The easiest way around this problem is to operate with a linearly polarized optical trap, with polarization vector aligned at the “magic angle” [88] and corresponding magic wavelength [89] for the  $^1S_0 \rightarrow ^3P_2$  transition. This allows intrastate coherence within the  $^3P_2$   $F = 9/2$  (and other  $F$  levels) manifold, and interstate (i.e., optical qubit) coherence between the  $^1S_0$  and  $^3P_2$   $F = 9/2$ . We can also mitigate motional effects via high-fidelity ground-state cooling [90–92].

#### IV. CONCLUSION AND OUTLOOK

Quantum computation with qudits has potential advantages when compared with architectures employing qubits. Implementing gates for qudit-based quantum computation is fundamentally more challenging, as the generators for these gates are not native Hamiltonians on physical platforms. One way to overcome this challenge is to use the tools of quantum optimal control, whereby we combine native Hamiltonians with time-dependent waveforms that drive the system in order to implement a universal gate set with high fidelity.

In this work, we introduced two classes of numerical methods of quantum optimal control for implementing the qudit entangling gates, an essential component of the universal gate set. The first approach is based on continuous-time driving given a controllable Hamiltonian with tunable parameters and uses the Lie algebraic structure of the control problem. The second approach is more “digital,” using

the Lie group structure to design a family of unitary maps that can be applied in sequence to achieve any nontrivial entangling gate of interest.

As a specific example, we studied encoding a qudit in the nuclear spin of  $^{87}\text{Sr}$ , a species of atoms that is particularly important in quantum information processing. The nuclear spin can accommodate a qudit of dimension  $d \leq 10$ . We have previously studied protocols for implementing single-qudit gates in  $SU(d)$ . To implement entangling gates we studied how we make two atoms interact using the well-known Rydberg blockade mechanism, and in particular, we studied Rydberg dressing schemes. Using this we are able to generate any two-qudit entangling gate, both using the Lie algebraic and Lie-group-based approaches.

We also studied how the fundamental effects of decoherence introduced by the finite lifetime of the Rydberg states reduce the gate fidelity. To model this we used a non-Hermitian Hamiltonian and found that even when including decoherence, one could achieve high fidelity for these qudit entanglers. Given the flexibility of arbitrary control, we can seek the best approach to encoding qudits and mitigating errors.

Finally, while we have studied a particular case study in the context of neutral-atom quantum computing, the general methods we have developed here can be applied in other platforms, including trap ions, transmon qudits, and nanomagnets [93,94], which also have natural encoding and control Hamiltonians.

#### ACKNOWLEDGMENTS

This work was supported by the Laboratory Directed Research and Development program of Los Alamos National Laboratory under Projects No. 20200015ER and No. 20210116DR, and the NSF Quantum Leap Challenge Institutes program, Award No. 2016244. The authors acknowledge fruitful discussions with Sri Datta Vikas Buchemavari, Milad Marvian, Pablo Poggi, Jonathan Gross, Irfan Siddiqi, and Noah Goss during various stages of this work.

#### APPENDIX A: HYPERFINE STRUCTURE OF RYDBERG STATES AND CLEBSCH-GORDAN COEFFICIENTS

As described in Sec. II C, to create entanglement we promote the population from the ground state  $^1S_0$  to the first excited  $^3P_2$  state, with the hyperfine quantum number  $F = 9/2$ , and then consider a UV laser to excite the atoms to the  $^3S_1$  Rydberg series to implement the interaction between atoms with adiabatic dressing (see Fig. 2). The Rabi frequency characterizing the coupling of the different  $m_F$  levels in the  $^3P_2$  hyperfine manifold to the  $^3S_1$  Rydberg states will be different due to the Clebsch-Gordan coefficients for these transitions. Let  $\Omega_L$  be the Rabi frequency on the  $|0_a\rangle \rightarrow |0_r\rangle$  ( $m_F = -9/2$  transition). The

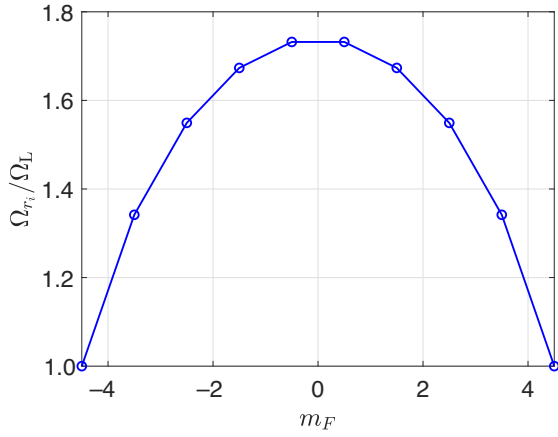


FIG. 7. Relative Rabi frequency,  $\Omega_{r_i}/\Omega_L$ , plotted as a function of  $m_F$  for  $\pi$  polarized light for the  $(5s5p)^3P_2F = 9/2 \rightarrow (5sns)^3S_1F' = 11/2$  transition to the Rydberg state. The quadratic function arises due to the tensor polarizability.

Rabi frequency experienced by the other levels is then

$$\Omega_{r_i} = \frac{\langle F, m_F = -9/2 + i | 1, 0; F', m_F = -9/2 + i \rangle}{\langle F, m_F = -9/2 | 1, 0; F', m_F = -9/2 \rangle} \Omega_L, \quad (\text{A1})$$

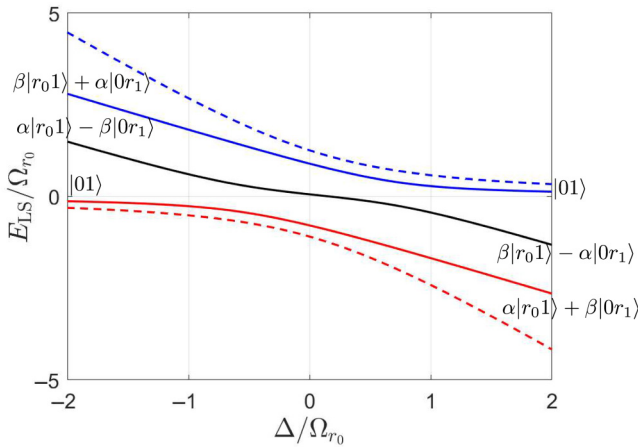


FIG. 8. Autler-Townes splitting of the three dressed states as a function of detuning for the Hamiltonian in Eq. (A2), where  $i = 0, j = 1$ , such that  $|0\rangle \equiv |^3P_2, m_F = 9/2\rangle$  and  $|1\rangle \equiv |^3P_2, m_F = 7/2\rangle$ . Here  $\alpha = \sqrt{7/16}$  and  $\beta = \sqrt{9/16}$ . The dashed line shows the ac Stark shift (light shift) in the absence of a perfect Rydberg blockade. The blue curve adiabatically connects to the clock states for large blue detuning and the red curve for large red detuning. The black curve is a dressed superposition that does not adiabatically connect to the clock states. The dashed lines show the light shifts in the absence of van der Waals interactions between the atoms. The difference between the solid line and the dashed line is the entangling power of the Hamiltonian  $H_2^{12}$  defined in Eq. (A2).

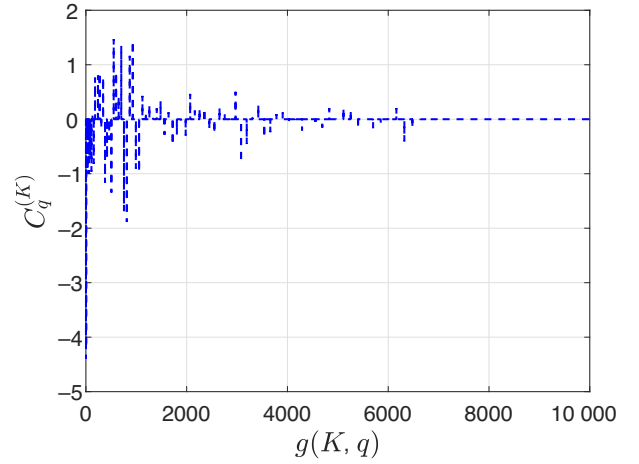


FIG. 9. The decomposition the entangling Hamiltonian  $H_{\text{ent}}$ , Eq. (5) in different orders of spherical tensors,  $T_q^{(K)}$ , for  $j = 99/2$ , an operator basis of dimension  $D = 2j + 1 = 100$ , spanning the two-qudit space for  $d = 10$ . The expansion coefficients are given by  $C_q^{(K)} = |\text{Tr}(H_{\text{ent}} T_q^{(K)\dagger})|^2$ . We have ordered the expansion coefficients according to  $g(K, q) = (k + 1)^2 - 1 + q$ , where  $0 \leq k \leq j$ , and  $-k \leq q \leq k$ . The existence of contributions from higher-rank tensors makes the system controllable when combined with time-dependent rf fields that act locally on the atoms.

where we have chosen  $F = 9/2$  and  $F' = 11/2$ , and a  $\pi$ -polarized light. In Fig. 7 the Rabi frequencies of the different levels are given as a function of  $m_F$ , whose parabolic shape describes the tensor light shift, thus giving a natural nonlinearity, which arises solely due to well-defined hyperfine structure of  $^{87}\text{Sr}$ .

Consider the Rydberg dressing scheme in Fig. 2. In the perfect blockade regime, the two-atom Hamiltonian coupling of two magnetic sublevels labeled  $i$  and  $j$  is described by a three-level system, governed by the Hamiltonian,

$$H_2^{ij} = -\Delta_i |r_j\rangle \langle r_j| + \frac{\Omega_{r_i}}{2} (|r_j\rangle \langle ij| + |ij\rangle \langle r_j|) - \Delta_j |ir_j\rangle \langle ir_j| + \frac{\Omega_{r_j}}{2} (|ir_j\rangle \langle ij| + |ij\rangle \langle ir_j|), \quad (\text{A2})$$

where  $\Delta_i$  determines the detunings due to the differential Zeeman shift. Figure 8 shows the resulting ac Stark shifts on the three dressed states after diagonalizing this Hamiltonian. The dressed ground state is shown in red; the other two dressed states represent Autler-Townes splitting. In the absence of the van der Waals interaction the ac Stark shift (light shift) is the sum of the light shifts of each atom independently (dashed line in Fig. 8). The difference between these is the entangling energy.

One can understand the entangling power of the Hamiltonian by studying the properties of the dressed energy levels as a function of detuning. Figure 8 shows the particular case of  $i = 0, j = 1$  for the Hamiltonian in Eq.

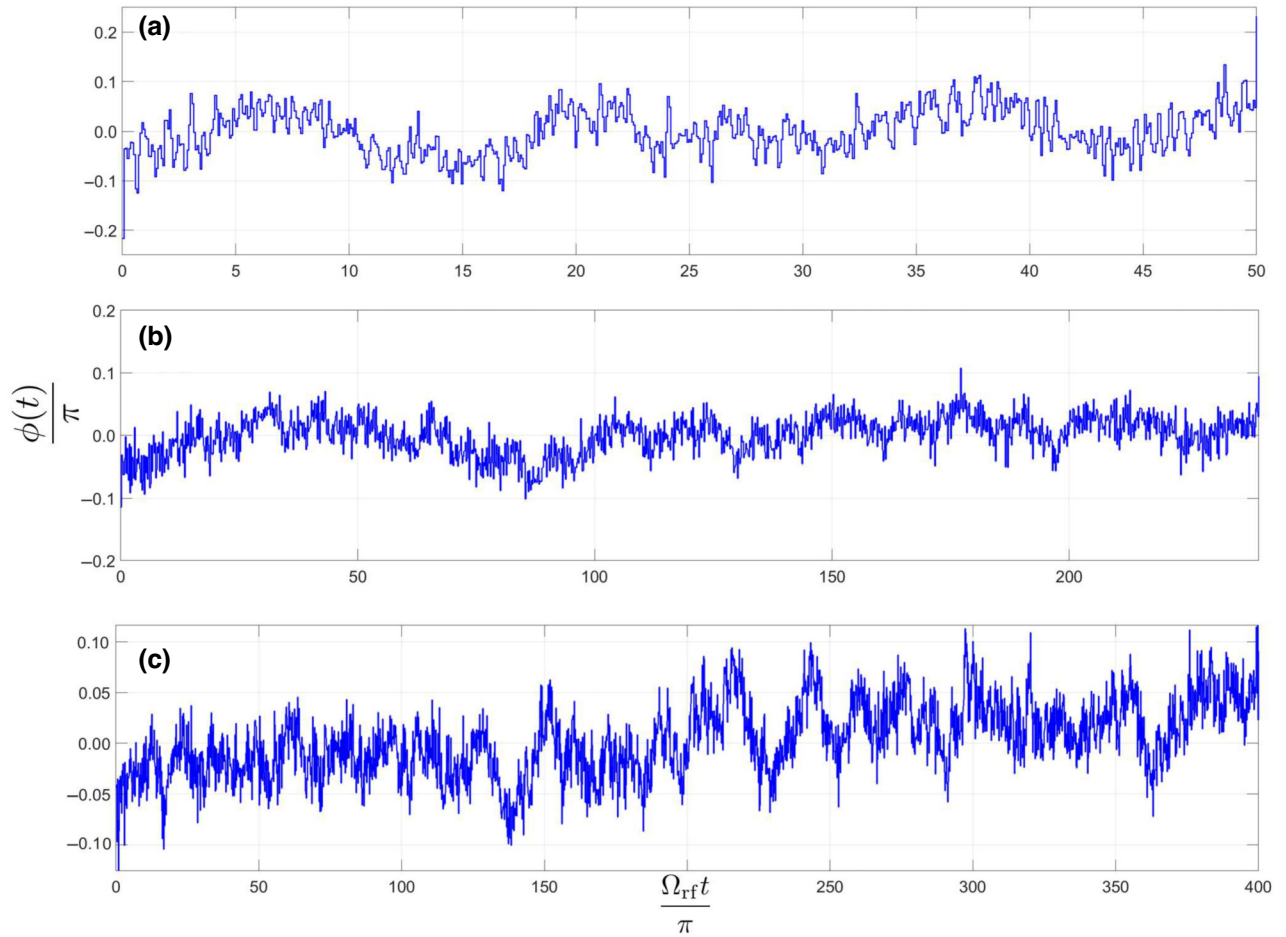


FIG. 10. The figure gives the  $\phi(t)$  that generates the Mølmer-Sørensen gate as a function of time for  $\theta = \pi/2$  using the piecewise constant quantum control approach for the Hamiltonian given in Eq. (5). In (a) the case of the  $d = 3$  for a total time of  $\Omega_{\text{rf}}T = 50\pi$  with 700 piecewise constant steps. In (b) the case of the  $d = 5$  for a total time of  $\Omega_{\text{rf}}T = 240\pi$  with 1600 piecewise constant steps. And in (c) the case of the  $d = 7$  for a total time of  $\Omega_{\text{rf}}T = 240\pi$  with 2500 piecewise constant steps. For all of these calculations we have taken  $\Omega_L = 6\Omega_{\text{rf}}$ .

(A2), where  $|0\rangle \equiv |m_F = 9/2\rangle$  and  $|1\rangle \equiv |m_F = 7/2\rangle$ . On the red side of detuning and for large detuning, as we start with the bare state and we adiabatically sweep through resonance, the state maps to the superposition of the two Rydberg states. Note, this is not an equal superposition as seen in Ref. [67] due to the fact that the states  $|0\rangle$  and  $|1\rangle$  couple with different Rydberg Rabi frequency and detuning to the Rydberg states.

## APPENDIX B: CONTROLLABILITY

The quantum system is said to be controllable if, given a time-dependent Hamiltonian  $H[\mathbf{c}(t)]$ , there exist a time-dependent set of waveforms  $\mathbf{c}(t)$ , such that the one can generate an arbitrary unitary map. Here we consider those two-qudit unitary maps generated by an entangling Hamiltonian that is symmetric under the exchange of the qudits and thus does not require local addressing. To show that a Hamiltonian is controllable, we use the operator basis of

irreducible spherical tensors on spin  $j$  defined as [95,96],

$$T_q^{(k)} = \sqrt{\frac{2k+1}{2j+1}} \sum_m \langle j, k+q | k, q; j, m \rangle |j, m+q\rangle \langle j, m|. \quad (\text{B1})$$

These satisfy the fundamental commutation relations,

$$\begin{aligned} [j_z, T_q^{(k)}] &= q T_q^{(k)}, \\ [j_{\pm}, T_q^{(k)}] &= \sqrt{k(k+1) - q(q \pm 1)} T_{q \pm 1}^{(k)}. \end{aligned} \quad (\text{B2})$$

The set of operators  $T_q^{(k)}$  form a complete orthonormal operator basis. Merkel *et al.* [80] showed that given a generating set of Hamiltonians  $\{h_i\}$ , if

$$\text{Tr}\{h_i, T_q^{(k)}\} \neq 0 \quad (\text{B3})$$

for  $k \geq 2$ , the system is fully controllable. That is, the set generates the whole Lie algebra of interest, which thus allows us to implement an arbitrary unitary map on the spin of the system using quantum control.

We consider two-qudit systems, where the relevant Lie group is  $SU(d^2)$ ; here  $d^2 = 100$ . We expand the entangling Hamiltonian in the operator basis of spherical tensors with  $j = 99/2$ , spanning the space of dimension  $D = 2j + 1 = 100$ . Figure 9 shows operator decomposition of the entangling Hamiltonian  $H_{\text{ent}}$  in different orders of spherical tensors. One can see in this figure that there are contributions from higher-rank tensors, making the system controllable.

### APPENDIX C: CREATING OTHER SYMMETRIC QUDIT ENTANGLERS FOR THE LIE ALGEBRAIC APPROACH

Since the Hamiltonian described in Eq. (3) can be used to create any symmetric two-qudit Hamiltonian, we can also generate the Mølmer-Sørensen gate for qudits defined as,

$$U_{\text{MS}}(\theta) = \exp\left(-i\theta \frac{J_z^2}{2}\right), \quad (\text{C1})$$

where the total angular momentum operator for the two qudits is

$$J_z = \mathbb{1} \otimes j_z + j_z \otimes \mathbb{1}. \quad (\text{C2})$$

We employ the same procedure for optimal control as we discussed in the main text in designing the waveforms to implement the CPhase gate. Numerical examples of the waveforms that create the Mølmer-Sørensen gate for  $\theta = \pi/2$  are given in Fig. 10. The figure shows  $\phi(t)$ , the piecewise constant of the control waveform, obtained using the GRAPE algorithm. Figure 3(a) shows the case of the  $k = 3$  the qutrit encoded in  $d = 10$ . The total time is  $T = 50\pi/\Omega_{\text{rf}}$  and we divide the time into 700 time steps for the quantum control. In Fig. 3(b) we plot an example waveform for the case of the  $d = 5$  into our ten-level system. We have a total time of  $T = 240\pi/\Omega_{\text{rf}}$  and we divide the time into 1600 time steps for the quantum control. In Fig. 3(c) we plot an example for the case of the  $d = 7$  into our ten-level system. We have a total time of  $T = 400\pi/\Omega_{\text{rf}}$  and we divide the time into 2500 time steps for the quantum control.

---

[1] Yuchen Wang, Zixuan Hu, Barry C. Sanders, and Sabre Kais, Qudits and high-dimensional quantum computing, *Front. Phys.* **8**, 589504 (2020).  
 [2] M. S. Blok, V. V. Ramasesh, T. Schuster, K. O'Brien, J. M. Kreikebaum, D. Dahlen, A. Morvan, B. Yoshida, N. Y.

Yao, and I. Siddiqi, Quantum information scrambling on a superconducting qutrit processor, *Phys. Rev. X* **11**, 021010 (2021).  
 [3] Jonathan A. Gross, Designing codes around interactions: The case of a spin, *Phys. Rev. Lett.* **127**, 010504 (2021).  
 [4] Shruti Puri, Lucas St-Jean, Jonathan A. Gross, Alexander Grimm, Nicholas E. Frattini, Pavithran S. Iyer, Anirudh Krishna, Steven Touzard, Liang Jiang, Alexandre Blais, Steven T. Flammia, and S. M. Girvin, Bias-preserving gates with stabilized cat qubits, *Sci. Adv.* **6**, eaay5901 (2020).  
 [5] Daniel Gottesman, Alexei Kitaev, and John Preskill, Encoding a qubit in an oscillator, *Phys. Rev. A* **64**, 012310 (2001).  
 [6] Mikio Fujiwara, Masahiro Takeoka, Jun Mizuno, and Masahide Sasaki, Exceeding the classical capacity limit in a quantum optical channel, *Phys. Rev. Lett.* **90**, 167906 (2003).  
 [7] Ming-Xing Luo, Xiu-Bo Chen, Yi-Xian Yang, and Xiaojun Wang, Geometry of quantum computation with qudits, *Sci. Rep.* **4**, 1 (2014).  
 [8] MingXing Luo and XiaoJun Wang, Universal quantum computation with qudits, *Sci. China Phys., Mech. Astron.* **57**, 1712 (2014).  
 [9] Bin Li, Zu-Huan Yu, and Shao-Ming Fei, Geometry of quantum computation with qutrits, *Sci. Rep.* **3**, 2594 (2013).  
 [10] Hsuan-Hao Lu, Zixuan Hu, Mohammed Saleh Alshaykh, Alexandria Jeanine Moore, Yuchen Wang, Poolad Imany, Andrew Marc Weiner, and Sabre Kais, Quantum phase estimation with time-frequency qudits in a single photon, *Adv. Quantum Technol.* **3**, 1900074 (2020).  
 [11] Shawn X. Cui and Zhenghan Wang, Universal quantum computation with metaplectic anyons, *J. Math. Phys.* **56**, 032202 (2015).  
 [12] Shawn X Cui, Seung-Moon Hong, and Zhenghan Wang, Universal quantum computation with weakly integral anyons, *Quantum Inf. Process.* **14**, 2687 (2015).  
 [13] Alex Bocharov, Shawn X. Cui, Martin Roetteler, and Krysta M. Svore, Improved quantum ternary arithmetics, arXiv preprint [arXiv:1512.03824](https://arxiv.org/abs/1512.03824) (2015).  
 [14] Jean-Luc Brylinski and Ranee Brylinski, Universal quantum gates, *Mathematics Quantum Computation* **79**, 117 (2002).  
 [15] V. E. Zbov and A. S. Ermilov, Implementation of a quantum adiabatic algorithm for factorization on two qudits, *J. Exp. Theor. Phys.* **114**, 923 (2012).  
 [16] Jordi R. Weggemans, Alexander Urech, Alexander Rausch, Robert Spreeuw, Richard Boucherie, Florian Schreck, Kareljan Schoutens, Jiří Minář, and Florian Speelman, Solving correlation clustering with QAOA and a Rydberg qudit system: a full-stack approach, *Quantum* **6**, 687 (2022).  
 [17] Daniel González-Cuadra, Torsten V. Zache, Jose Carrasco, Barbara Kraus, and Peter Zoller, Hardware efficient simulation of non-Abelian gauge theories with qudits on Rydberg platforms, *Phys. Rev. Lett.* **129**, 160501 (2022).  
 [18] Earl T. Campbell, Enhanced fault-tolerant quantum computing in  $d$ -level systems, *Phys. Rev. Lett.* **113**, 230501 (2014).

- [19] Wim van Dam and Mark Howard, Noise thresholds for higher-dimensional systems using the discrete Wigner function, *Phys. Rev. A* **83**, 032310 (2011).
- [20] Daniel Gottesman, in *Quantum Computing and Quantum Communications*, edited by Colin P. Williams (Springer Berlin Heidelberg, Berlin, Heidelberg, 1999), p. 302.
- [21] Earl T. Campbell, Hussain Anwar, and Dan E. Browne, Magic-state distillation in all prime dimensions using quantum Reed-Muller codes, *Phys. Rev. X* **2**, 041021 (2012).
- [22] Eliot Kapit, Hardware-efficient and fully autonomous quantum error correction in superconducting circuits, *Phys. Rev. Lett.* **116**, 150501 (2016).
- [23] Austin G. Fowler, Matteo Mariantoni, John M. Martinis, and Andrew N. Cleland, Surface codes: Towards practical large-scale quantum computation, *Phys. Rev. A* **86**, 032324 (2012).
- [24] Sivaprasad Omanakuttan and Jonathan Gross, Multispin Clifford codes for angular momentum errors in spin systems, arXiv preprint [arXiv:2304.08611](https://arxiv.org/abs/2304.08611) (2023).
- [25] Victor V. Albert, Jacob P. Covey, and John Preskill, Robust encoding of a qubit in a molecule, *Phys. Rev. X* **10**, 031050 (2020).
- [26] Jonathan A. Gross, Clément Godfrin, Alexandre Blais, and Eva Dupont-Ferrier, Hardware-efficient error-correcting codes for large nuclear spins, arXiv preprint [arXiv:2103.08548](https://arxiv.org/abs/2103.08548) (2021).
- [27] David P. DiVincenzo, Two-bit gates are universal for quantum computation, *Phys. Rev. A* **51**, 1015 (1995).
- [28] Ashok Muthukrishnan and C. R. Stroud, Multivalued logic gates for quantum computation, *Phys. Rev. A* **62**, 052309 (2000).
- [29] D. L. Zhou, B. Zeng, Z. Xu, and C. P. Sun, Quantum computation based on d-level cluster state, *Phys. Rev. A* **68**, 062303 (2003).
- [30] Gavin K. Brennen, Dianne P. O’Leary, and Stephen S. Bullock, Criteria for exact qudit universality, *Phys. Rev. A* **71**, 052318 (2005).
- [31] Noah Goss, Alexis Morvan, Brian Marinelli, Bradley K. Mitchell, Long B. Nguyen, Ravi K. Nail, Larry Chen, Christian Jünger, John Mark Kreikebaum, and David I. Santiago *et al.*, High-fidelity qutrit entangling gates for superconducting circuits, arXiv preprint [arXiv:2206.07216](https://arxiv.org/abs/2206.07216) (2022), 10.48550/arXiv.2206.07216.
- [32] Laurin E. Fischer, Alessandro Chiesa, Francesco Tacchino, Daniel J. Egger, Stefano Carretta, and Ivano Tavernelli, Towards universal gate synthesis and error correction in transmon qudits, arXiv preprint [arXiv:2212.04496](https://arxiv.org/abs/2212.04496) (2022), 10.48550/arXiv.2212.04496.
- [33] Martin Ringbauer, Michael Meth, Lukas Postler, Roman Stricker, Rainer Blatt, Philipp Schindler, and Thomas Monz, A universal qudit quantum processor with trapped ions, *Nat. Phys.* **18**, 1053 (2022).
- [34] Pavel Hřmó, Benjamin Wilhelm, Lukas Gerster, Martin W. van Mourik, Marcus Huber, Rainer Blatt, Philipp Schindler, Thomas Monz, and Martin Ringbauer, Native qudit entanglement in a trapped ion quantum processor, arXiv preprint [arXiv:2206.04104](https://arxiv.org/abs/2206.04104) (2022).
- [35] Chi-Kwong Li, Rebecca Roberts, and Xiaoyan Yin, Decomposition of unitary matrices and quantum gates, *Int. J. Quantum Inf.* **11**, 1350015 (2013).
- [36] L. M. K. Vandersypen and I. L. Chuang, NMR techniques for quantum control and computation, *Rev. Mod. Phys.* **76**, 1037 (2005).
- [37] Herschel Rabitz, Regina de Vivie-Riedle, Marcus Motzkus, and Karl Kompa, Whither the future of controlling quantum phenomena?, *Science* **288**, 824 (2000).
- [38] *Quantum Control of Molecular Processes* (John Wiley & Sons, Ltd, 2011), Chap. 17, p. 463. <https://onlinelibrary.wiley.com/doi/abs/10.1002/9783527639700.ch17>.
- [39] Christiane P. Koch, Ugo Boscain, Tommaso Calarco, Gunther Dirr, Stefan Filipp, Steffen J. Glaser, Ronnie Kosloff, Simone Montangero, Thomas Schulte-Herbrüggen, Dominique Sugny, and Frank K. Wilhelm, Quantum optimal control in quantum technologies. strategic report on current status, visions and goals for research in Europe, *EPJ Quantum Technol.* **9**, 19 (2022).
- [40] Uffe V. Poulsen, Shlomo Sklarz, David Tannor, and Tommaso Calarco, Correcting errors in a quantum gate with pushed ions via optimal control, *Phys. Rev. A* **82**, 012339 (2010).
- [41] Philipp Treutlein, Theodor W. Hänsch, Jakob Reichel, Antonio Negretti, Markus A. Cirone, and Tommaso Calarco, Microwave potentials and optimal control for robust quantum gates on an atom chip, *Phys. Rev. A* **74**, 022312 (2006).
- [42] Michael H. Goerz, Eli J. Halperin, Jon M. Aytac, Christiane P. Koch, and K. Birgitta Whaley, Robustness of high-fidelity Rydberg gates with single-site addressability, *Phys. Rev. A* **90**, 032329 (2014).
- [43] Nathan K. Lysne, Kevin W. Kuper, Pablo M. Poggi, Ivan H. Deutsch, and Poul S. Jessen, Small, highly accurate quantum processor for intermediate-depth quantum simulations, *Phys. Rev. Lett.* **124**, 230501 (2020).
- [44] P. Rebentrost, I. Serban, T. Schulte-Herbrüggen, and F. K. Wilhelm, Optimal control of a qubit coupled to a non-Markovian environment, *Phys. Rev. Lett.* **102**, 090401 (2009).
- [45] Michael H. Goerz, Daniel M. Reich, and Christiane P. Koch, Optimal control theory for a unitary operation under dissipative evolution, *New J. Phys.* **16**, 055012 (2014).
- [46] Gerald Waldherr, Y. Wang, S. Zaiser, M. Jamali, T. Schulte-Herbrüggen, H. Abe, T. Ohshima, J. Isoya, J. F. Du, P. Neumann, and J. Wrachtrup, Quantum error correction in a solid-state hybrid spin register, *Nature* **506**, 204 (2014).
- [47] Jochen Scheuer, Xi Kong, Ressa S. Said, Jenson Chen, Andrea Kurz, Luca Marseglia, Jiangfeng Du, Philip R. Hemmer, Simone Montangero, Tommaso Calarco, Boris Naydenov, and Fedor Jelezko, Precise qubit control beyond the rotating wave approximation, *New J. Phys.* **16**, 093022 (2014).
- [48] Brian Eric Anderson, Unitary transformations in a large Hilbert space, (2013).
- [49] Sivaprasad Omanakuttan, Anupam Mitra, Michael J. Martin, and Ivan H. Deutsch, Quantum optimal control of ten-level nuclear spin qudits in  $^{87}\text{Sr}$ , *Phys. Rev. A* **104**, L060401 (2021).
- [50] Katrina Barnes *et al.*, Assembly and coherent control of a register of nuclear spin qubits, *Nat. Commun.* **13**, 1 (2022).

- [51] Andrew J. Daley, Martin M. Boyd, Jun Ye, and Peter Zoller, Quantum computing with alkaline-earth-metal atoms, *Phys. Rev. Lett.* **101**, 170504 (2008).
- [52] Andrew J. Daley, Quantum computing and quantum simulation with group-II atoms, *Quantum Inf. Process.* **10**, 865 (2011).
- [53] Torsten V. Zache, Daniel González-Cuadra, and Peter Zoller, Fermion-qudit quantum processors for simulating lattice gauge theories with matter, arXiv preprint [arXiv:2303.08683](https://arxiv.org/abs/2303.08683) (2023).
- [54] Harry Levine, Alexander Keesling, Giulia Semeghini, Ahmed Omran, Tout T. Wang, Sepehr Ebadi, Hannes Bernien, Markus Greiner, Vladan Vuletić, Hannes Pichler, and Mikhail D. Lukin, Parallel implementation of high-fidelity multiqubit gates with neutral atoms, *Phys. Rev. Lett.* **123**, 170503 (2019).
- [55] Dolev Bluvstein, Harry Levine, Giulia Semeghini, Tout T. Wang, Sepehr Ebadi, Marcin Kalinowski, Alexander Keesling, Nishad Maskara, Hannes Pichler, Markus Greiner, Vladan Vuletić, Mikhail D. Lukin, and A quantum processor based on coherent transport of entangled atom arrays, *Nature* **604**, 451 (2022).
- [56] T. M. Graham *et al.*, Multi-qubit entanglement and algorithms on a neutral-atom quantum computer, *Nature* **604**, 457 (2022).
- [57] Navin Khaneja, Timo Reiss, Cindie Kehlet, Thomas Schulte-Herbrüggen, and Steffen J. Glaser, Optimal control of coupled spin dynamics: Design of NMR pulse sequences by gradient ascent algorithms, *J. Magn. Reson.* **172**, 296 (2005).
- [58] Alexander Yu Vlasov, Noncommutative tori and universal sets of nonbinary quantum gates, *J. Math. Phys.* **43**, 2959 (2002).
- [59] Raneë K. Brylinski and Goong Chen, *Mathematics of Quantum Computation* (CRC Press, New York, 2002).
- [60] J. E. Johnson and S. L. Rolston, Interactions between Rydberg-dressed atoms, *Phys. Rev. A* **82**, 033412 (2010).
- [61] Tyler Keating, Robert L. Cook, Aaron M. Hankin, Yuan-Yu Jau, Grant W. Biedermann, and Ivan H. Deutsch, Robust quantum logic in neutral atoms via adiabatic Rydberg dressing, *Phys. Rev. A* **91**, 012337 (2015).
- [62] Y.-Y. Jau, A. M. Hankin, T. Keating, I. H. Deutsch, and G. W. Biedermann, Entangling atomic spins with a Rydberg-dressed spin-flip blockade, *Nat. Phys.* **12**, 71 (2016).
- [63] Johannes Zeiher, Rick Van Bijnen, Peter Schauß, Sebastian Hild, Jae-yoon Choi, Thomas Pohl, Immanuel Bloch, and Christian Gross, Many-body interferometry of a Rydberg-dressed spin lattice, *Nat. Phys.* **12**, 1095 (2016).
- [64] Johannes Zeiher, Jae-yoon Choi, Antonio Rubio-Abadal, Thomas Pohl, Rick van Bijnen, Immanuel Bloch, and Christian Gross, Coherent many-body spin dynamics in a long-range interacting Ising chain, *Phys. Rev. X* **7**, 041063 (2017).
- [65] V. Borish, O. Marković, J. A. Hines, S. V. Rajagopal, and M. Schleier-Smith, Transverse-field Ising dynamics in a Rydberg-dressed atomic gas, *Phys. Rev. Lett.* **124**, 063601 (2020).
- [66] Raphael Kaubruegger, Pietro Silvi, Christian Kokail, Rick van Bijnen, Ana Maria Rey, Jun Ye, Adam M. Kaufman, and Peter Zoller, Variational spin-squeezing algorithms on programmable quantum sensors, *Phys. Rev. Lett.* **123**, 260505 (2019).
- [67] Anupam Mitra, Michael J. Martin, Grant W. Biedermann, Alberto M. Marino, Pablo M. Poggi, and Ivan H. Deutsch, Robust Mølmer-Sørensen gate for neutral atoms using rapid adiabatic rydberg dressing, *Phys. Rev. A* **101**, 030301 (2020).
- [68] Anupam Mitra, Sivaprasad Omanakuttan, Michael J. Martin, Grant W. Biedermann, and Ivan H. Deutsch, Practical and fundamental limits of neutral atom entanglement using rydberg dressing arXiv preprint [arXiv:2205.12866](https://arxiv.org/abs/2205.12866) (2022).
- [69] Michael J. Martin, Yuan-Yu Jau, Jongmin Lee, Anupam Mitra, Ivan H. Deutsch, and Grant W. Biedermann, A Mølmer-Sørensen gate with Rydberg-dressed atoms, arXiv e-prints, arXiv:2111 (2021), doi:10.48550/arXiv.2111.14677.
- [70] Nathan Schine, Aaron W. Young, William J. Eckner, Michael J. Martin, and Adam M. Kaufman, Long-lived bell states in an array of optical clock qubits, *Nat. Phys.* **18**, 1067 (2022).
- [71] Vikas Buchemavari, Sivaprasad Omanakuttan, Yuan-Yu Jau, and Ivan Deutsch, Entangling quantum logic gates in neutral atoms via the microwave-driven spin-flip blockade, arXiv preprint [arXiv:2307.16434](https://arxiv.org/abs/2307.16434) (2023).
- [72] Jan Trautmann, Dimitry Yankelev, Valentin Klüsener, Annie Ji Hyun Park, Immanuel Bloch, and Sebastian Blatt, The  $1S_0 - 3P_2$  magnetic quadrupole transition in neutral strontium, arXiv preprint [arXiv:2211.02470](https://arxiv.org/abs/2211.02470) (2022).
- [73] Line Hjortshøj Pedersen, Niels Martin Møller, and Klaus Mølmer, Fidelity of quantum operations, *Phys. Lett. A* **367**, 47 (2007).
- [74] J. Sutherland Frame, G. de B. Robinson, and Robert M. Thrall, The hook graphs of the symmetric group, *Can. J. Mathematics* **6**, 316 (1954).
- [75] Shai Machnes, Elie Assémat, David Tannor, and Frank K. Wilhelm, Tunable, flexible, and efficient optimization of control pulses for practical qubits, *Phys. Rev. Lett.* **120**, 150401 (2018).
- [76] Martín Larocca, Pablo Poggi, and Diego Wisniacki, Quantum optimal control: Landscape structure and topology, arXiv preprint [arXiv:1802.05683](https://arxiv.org/abs/1802.05683) (2018).
- [77] Alexandre Choquette, Agustin Di Paolo, Panagiotis Kl. Barkoutsos, David Sénéchal, Ivano Tavernelli, and Alexandre Blais, Quantum-optimal-control-inspired ansatz for variational quantum algorithms, *Phys. Rev. Res.* **3**, 023092 (2021).
- [78] Hussain Anwar, Benjamin J. Brown, Earl T. Campbell, and Dan E. Browne, Fast decoders for qudit topological codes, *New J. Phys.* **16**, 063038 (2014).
- [79] Fern H. E. Watson, Hussain Anwar, and Dan E. Browne, Fast fault-tolerant decoder for qubit and qudit surface codes, *Phys. Rev. A* **92**, 032309 (2015).
- [80] Seth Merkel, Quantum control of d-dimensional quantum systems with application to alkali atomic spins, arXiv preprint [arXiv:0906.4790](https://arxiv.org/abs/0906.4790) (2009), 10.48550/arXiv.0906.4790.
- [81] Velimir Jurdjevic and Héctor J. Sussmann, Control systems on Lie groups, *J. Differ. Equ.* **12**, 313 (1972).
- [82] Roger W. Brockett, Lie theory and control systems defined on spheres, *SIAM J. Appl. Math.* **25**, 213 (1973).

- [83] B. E. Anderson, H. Sosa-Martinez, C. A. Riofrío, Ivan H. Deutsch, and Poul S. Jessen, Accurate and robust unitary transformations of a high-dimensional quantum system, *Phys. Rev. Lett.* **114**, 240401 (2015).
- [84] Michael Hartmut Goerz, *Optimizing robust quantum gates in open quantum systems*, Ph.D. thesis, 2015.
- [85] Steffen J. Glaser, Ugo Boscain, Tommaso Calarco, Christiane P. Koch, Walter Köckenberger, Ronnie Kosloff, Ilya Kuprov, Burkhard Luy, Sophie Schirmer, Thomas Schulte-Herbrüggen, Dominique Sugny, and Frank K. Wilhelm Training Schrödinger's cat: Quantum optimal control, *The European Physical Journal D* **69**, 1 (2015).
- [86] Christiane P. Koch, Controlling open quantum systems: Tools, achievements, and limitations, *J. Phys.: Condens. Matter* **28**, 213001 (2016).
- [87] J. Trautmann, D. Yankelev, V. Klüsener, A. J. Park, I. Bloch, and S. Blatt,  $^1S_0-^3P_2$  magnetic quadrupole transition in neutral strontium, *Phys. Rev. Res.* **5**, 013219 (2023).
- [88] M. A. Norcia, A. W. Young, and A. M. Kaufman, Microscopic control and detection of ultracold strontium in optical-tweezer arrays, *Phys. Rev. X* **8**, 041054 (2018).
- [89] Jun Ye, H. J. Kimble, and Hidetoshi Katori, Quantum state engineering and precision metrology using state-insensitive light traps, *Science* **320**, 1734 (2008).
- [90] Adam M. Kaufman, Brian J. Lester, and Cindy A. Regal, Cooling a single atom in an optical tweezer to its quantum ground state, *Phys. Rev. X* **2**, 041014 (2012).
- [91] Jeffrey Douglas Thompson, T. G. Tiecke, Alexander S. Zibrov, V. Vuletić, and Mikhail D. Lukin, Coherence and Raman sideband cooling of a single atom in an optical tweezer, *Phys. Rev. Lett.* **110**, 133001 (2013).
- [92] Brian J. Lester, Adam M. Kaufman, and Cindy A. Regal, Raman cooling imaging: Detecting single atoms near their ground state of motion, *Phys. Rev. A* **90**, 011804 (2014).
- [93] Francesco Petiziol, Alessandro Chiesa, Sandro Wimberger, Paolo Santini, and Stefano Carretta, Counteracting dephasing in molecular nanomagnets by optimized qudit encodings, *Npj Quantum Inf.* **7**, 133 (2021).
- [94] A. Chiesa, F. Petiziol, E. Macaluso, S. Wimberger, P. Santini, and S. Carretta, Embedded quantum-error correction and controlled-phase gate for molecular spin qubits, *AIP Adv.* **11**, 025134 (2021).
- [95] J Sakurai and J Napolitano, "Modern quantum mechanics. 2-nd edition," Person New International edition (2014).
- [96] A. B. Klimov and P Espinoza, Moyal-like form of the star product for generalized SU(2) Stratonovich-Weyl symbols, *J. Phys. A: Math. Gen.* **35**, 8435 (2002).